Seamless X100 Low-Carbon Steel Grade for Offshore Structural Applications

Authors

José Francisco Maranho, Vallourec South America, Distrito Industrial, Jeceaba, MG, Brazil
jose.maranho@vallourec.com

Diego de Araujo Santana, Vallourec South America, Distrito Industrial, Jeceaba, MG, Brazil
diego.santana@vallourec.com

Vicente Braz Trindade, Vallourec South America, Distrito Industrial, Jeceaba, MG, Brazil
vicente.trindade@vallourec.com

High-strength low-alloy steels have been widely used worldwide in offshore structural applications like jack-up rigs and wind turbine installation vessels. With rising demand for materials with higher mechanical strength, the X100Q grade, a C-Mn steel with low carbon content and a well-balanced microalloying concept, has emerged as a promising candidate. In this work, steel bars were hot-rolled to produce seamless pipes, which were then quenched and tempered. Microstructural characterization of the pipe revealed a microstructure consisting of bainite and tempered martensite. Mechanical characterization demonstrated that the material has a good combination of high strength and toughness in temperatures as low as –60°C.

Introduction

Jack-up rigs (JuR) and wind turbine installation vessels (WTIV) are self-elevating platforms. The former is used for oil and gas exploration in shallow waters,[1] as shown in Fig. 1a. The latter is used for offshore wind farms construction,[2,3] as displayed in Fig. 1b. The increasing global demand for these applications, particularly in harsh environmental conditions characterized by water currents, storm loads, waves and low temperatures, requires that the steel used in JuR and WTIV presents a suitable compromise of high mechanical strength and toughness.

Based on that, high-strength low-alloy steel (HSLA) is a common choice for such offshore structural applications, and a potential candidate is X100 grade, commonly applied in pipelines[6–8] but also evaluated for offshore applications.[9–11] The main usage of HSLA in the JuR and WTIV is in the trussed legs and trussed cranes. HSLA presents a combination of high strength, formability and weldability. These are key properties to guarantee a safe construction and operation of offshore structural

Figure 1

Main applications of X100Q grade: Jack-up rigs[4] (a) and wind turbine installation vessel (b).[5]

(a) (b)

Table 1

Limits of the Steel Chemistry (wt. %)

C	Mn	Si	Cr	Mo	Ni	Nb + V + Ti	B	CE_{IIW}	P_{CM}
≤0.100	≤1.500	≤0.500	≤0.500	≤0.500	≤1.000	≤0.150	≤0.005	≤0.570	≤0.280

applications. A well-balanced microalloying concept in the steel's chemistry combined with a proper heat treatment is essential to achieve the desired microstructure and mechanical properties of the final product.

In this study, low-carbon seamless steel pipes of grade X100Q , equivalent to grades from ABS Rules for Materials and Welding – Part 2[12] and DNV-OS-B101[13] standards for offshore structural applications, were produced and had their mechanical properties evaluated through tensile, hardness and impact tests. The microstructure of the pipes was characterized through light optical microscopy (LOM) and scanning electron microscopy (SEM).

Figure 2

Seamless pipe manufacturing: Pipe after exiting premium quality finishing (PQF) rolling mill (a) and before starting quenching (b).

(a) (b)

Materials and Methods

Seamless pipes were produced from continuously cast billets at Vallourec South America, in Jeceaba, Brazil. The limits of the chemical composition of the studied steel, the equivalent carbon (CE_{IIW}) and the critical metal parameter (P_{CM}) are summarized in Table 1. The CE_{IIW} and P_{CM} can be calculated using Eqs. 1 and 2, respectively.

$$CE_{IIW} = C + \frac{Mn}{6} + \frac{Cr + Mo + V}{5} + \frac{Ni + Cu}{15} \quad \text{(Eq. 1)}$$

$$P_{cm} = C + \frac{Si}{30} + \frac{Mn + Cu + Cr}{20} + \frac{Ni}{60} + \frac{Mo}{15} + \frac{V}{10} + 5B \quad \text{(Eq. 2)}$$

For this study, 406 mm in diameter bars were hot-rolled into three pipe dimensions. All pipes had an outside diameter (OD) of 355.6 mm, but wall thicknesses (WT) of 27.8, 30 and 40 mm. After rolling, the pipes were austenitized in a walking beam furnace at temperatures higher than 900°C. The quenching process was carried out in a water tank equipped with an internal water jet as well as an external lateral water jet, as shown in Fig. 2b. After quenching, the pipes were tempered at temperatures higher than 600°C.

Microstructural characterization of the pipes was conducted through LOM and SEM. For these analyses, the samples were ground and polished, following standard metallography procedures, and etched with Nital 3%.

The hardenability of the steel was assessed by means of Jominy tests as specified by ASTM A255-10.[14] Tensile tests were performed at room temperature in accordance with ASTM A370-23.[15] The specimens were machined both with their main axis parallel and transversal to the rolling direction. Charpy V-Notch (CVN) impact tests were carried out at –60, –40, –20 and 0°C, using full size standard specimen (10 x 10 x 55 mm), in accordance with ASTM E23-23.[16] The samples for CVN tests were machined from the pipe mid-wall with their main axis perpendicular to the rolling direction. Vickers hardness tests were performed, according to ASTM E92-23,[17] in the outer surface, mid-wall, and inner surface of the pipes in as-quenched and in as-quenched and tempered (QT) conditions.

Figure 3

Hardness HV10 as a function of distance from the quenched end after Jominy tests.

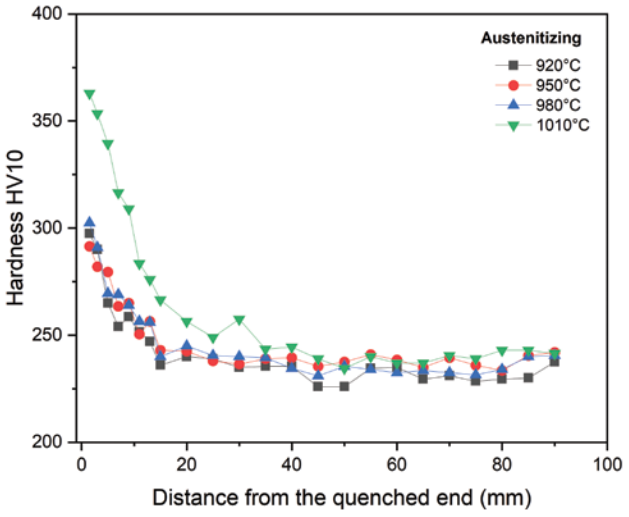

Results and Discussion

Hardenability results for specimens austenitized at different temperatures are shown in Fig. 3.

As it can be observed, higher austenitizing temperature leads to a higher hardenability of the material. This behavior is directly correlated to the prior austenite grain size (PAGS). With increasing temperature, a coarsening of austenite grain size occurs. Consequently, the grain boundary per unit volume decreases. Therefore, in terms of a continuous cooling transformation (CCT) diagram, the transformation curves tend to shift for higher times as the austenitic grain size increases, favoring the formation of martensite due to less nucleation site for diffusional phases. For the first three lowest austenitizing temperatures, the hardness plateau, around 240 HV10, starts at a depth of 20 mm, whereas for 1,010°C it starts at 35 mm. Since the application for this steel grade is in trussed structures, where the weldability is extremely important, the hardenability shall be controlled, and the low-carbon content combined with a well-balanced content of molybdenum, manganese, nickel and copper provides the necessary hardenability for this steel without jeopardizing its weldability.

Histograms of hardness in the as-quenched and as-QT (quenched and tempered) conditions for pipes with WT of 27.8, 30 and 40 mm are shown in Figs. 4a and 4b, respectively. The hardness was measured on different pipes positions along their lengths (leading end, middle and trailing end) as well as on different position along their cross-section (outer diameter, mid-wall and inner diameter).

It can be seen that the hardness values in the as-quenched condition, Fig. 4a, is on the same range of hardness observed in the Jominy tests. The higher mean hardness was achieved for WT 27.8, which is expected since the mean cooling rate along the wall thickness is higher as thinner the wall thickness is. In general, the hardness results were satisfactory, with most of the values above 300 HV10.

Regarding the as-QT condition, the results were quite homogeneous, with an average of 279, 283 and 275 HV10 for WTs 27.8, 30 and 40 mm, respectively. According to ABS standard, for the equivalent grade of X100Q, the hardness results shall not exceed 420 HV10 on base metal

Figure 4

Histogram of normal distribution for hardness measurements: Hardenability results from industrial quenching (a) and HV10 in as-quenched and tempered condition (b).

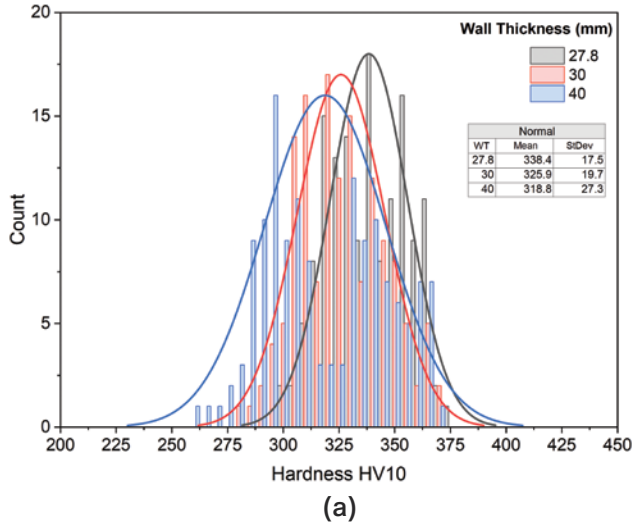

and 350 HV10 after welding. Based on that, the results were below the values of both specifications, with a good safety margin.

Figs. 5a and 5b show histograms of yield strength and ultimate tensile strength, respectively, measured in specimens extracted along the longitudinal direction of the pipes. On the other hand, Figs. 5c and 5d display the histograms of yield strength and ultimate tensile strength, respectively, and transverse direction. The dashed red lines in the graphs represent the requirements for the properties according to DNV OS-B101 and ABS Materials and Welding – Part 2. In terms of yield strength (YS), the minimum value is 690 MPa, and for ultimate tensile strength (UTS) the range varies from 770 to 940 MPa.

As shown in Fig. 5, the requirements were safely achieved for both test directions. For longitudinal direction, the YS varied from 705 to 810 MPa, and UTS from 780 to 870 MPa considering the three WTs evaluated in this study. For WT 40 mm, the values were slightly lower in comparison to WTs 27.8 and 30 mm. This behavior is already expected since the cooling rate at the mid-wall decreases as the wall thickness increases. For transverse direction, YS varied from 730 to 810 MPa, almost the same level of the longitudinal, and UTS varied from 820 to 870 MPa, considering the three WTs. Therefore, a good range of YS and UTS was obtained to achieve X100Q grade, fully in accordance with the standards.

The evolution of the microstructure of the pipe through the heat treatment is shown in Fig. 6. The microstructure of the pipes in the as-rolled condition is shown in

Figure 5

Histogram of distribution for tensile properties: Yield strength (YS) (a) and ultimate tensile strength (UTS) (b) in longitudinal direction, and YS (c) and UTS (d) in transverse direction.

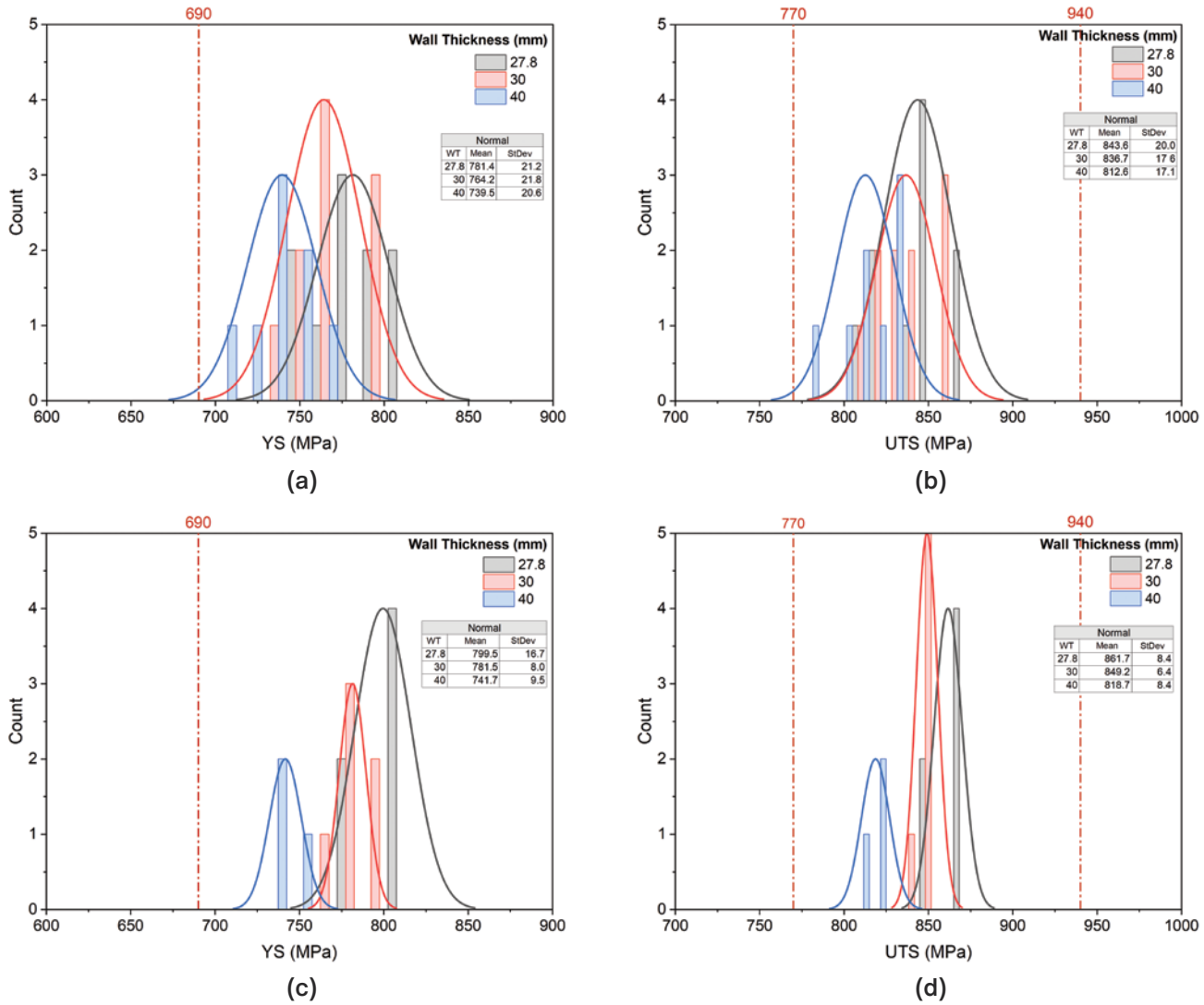

Figure 6

Microstructural evolution for X100Q grade. Light optical microscopy (LOM) images for the microstructure in as-rolled (a) and (b), as-quenched (c) and (d), and as-QT conditions (e) and (f); SEM images of as-QT condition (g) and (h).

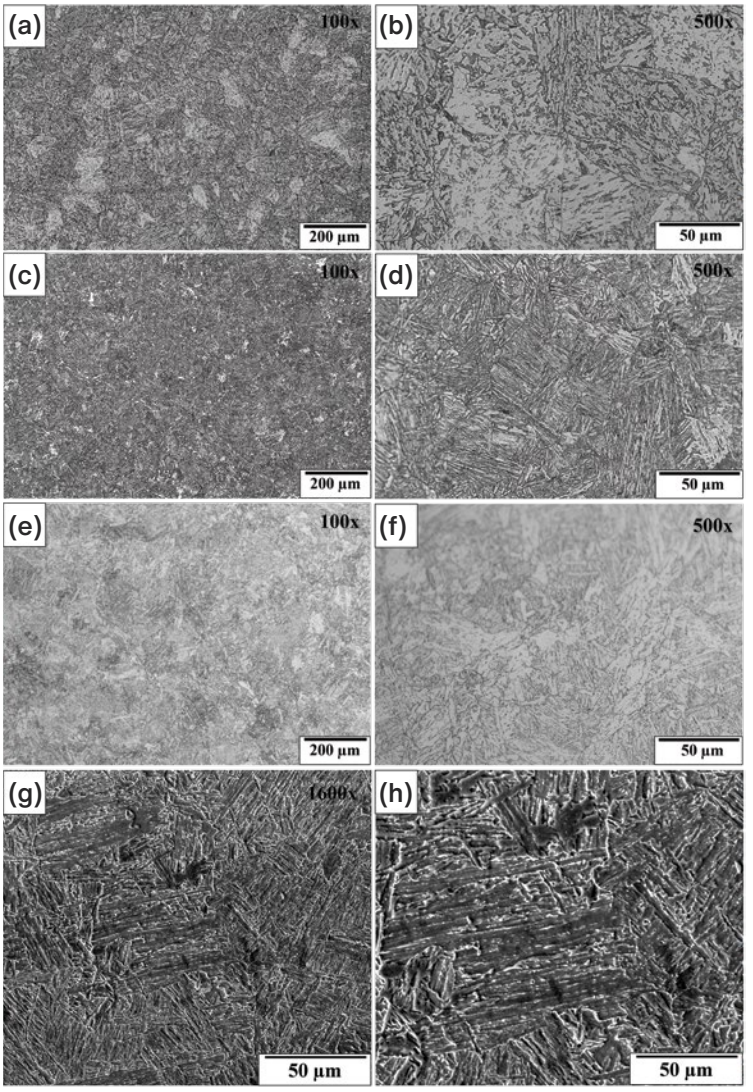

Figs. 6a and 6b. The microstructure of the pipes in the as-quenched condition is displayed in Figs. 6c and 6d. The microstructures in the as-QT conditions are shown in Figs. 6e and 6f. The sample in this latter condition was also characterized by means of SEM. Figs. 6g and 6h shows images acquired using the secondary electron detector.

In the as-rolled condition, the microstructure is mainly composed of bainite. Since the rolling temperature is around 1,100°C and the alloying concept has some elements for increasing the steel's hardenability, it is expected to obtain this kind of microstructure, even after the pipe being cooled to room temperature. For the as-quenched condition, Figs. 6c and 6d, the microstructure is mostly

Figure 7

Volume fraction of phases using thermodynamic simulation of equilibrium composition for steel chemistry applied to develop X100Q grade.

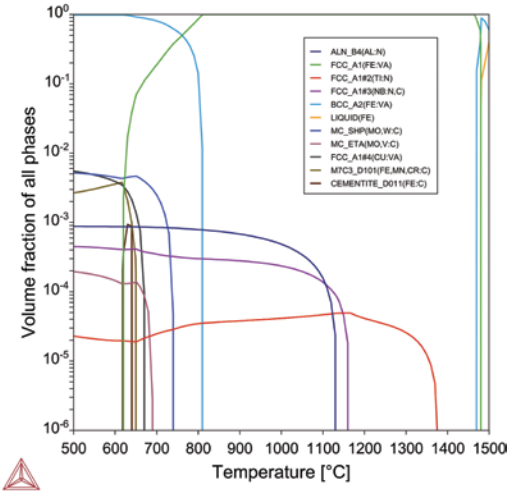

constituted of bainite with a few islands of lath martensite, a microstructure typical of low-carbon steels. After quenching and tempering, it is possible to observe mainly refined tempered bainite with few tempered martensite, corroborating with the previous microstructure obtained after quenching. Figs. 6g and 6h show SEM images obtained in as-QT condition, where very refined precipitates can be seen inside and between bainite plates.

Thermodynamic simulation was performed using Thermo-Calc software for the equilibrium composition. The main precipitates for grain boundary pinning at high temperatures and low-temperature precipitates formed during tempering are shown in Fig. 7.

It is possible to observe that the first precipitates to be formed are TiN, Nb (C,N) and AlN at 1,375°C, 1,160° and 1,125°C, respectively. It is well known that these precipitates formed at high temperatures are responsible for pinning the grain boundaries, refining them and improving mechanical strength and toughness. Furthermore, based on the dissolution temperatures of these precipitates, the austenitizing temperature applied in the heat treatment seems suitable, since they are stable at the temperature that was used. Around 800°C, the transformation from austenite to α-ferrite starts and decreasing the temperature, the low-temperature precipitates such Mo, V, W, Cr and Mn carbides start to be formed as well as Fe_3C, which is the main precipitate to strengthen the steel matrix for this material grade.

Figure 8

Charpy V-Notch (CVN) impact tests results for different temperatures for the evaluated wall thicknesses: Absorbed energy, longitudinal direction (a) and shear area for longitudinal direction (b), absorbed energy, transverse direction (c) and shear area for transverse direction (d).

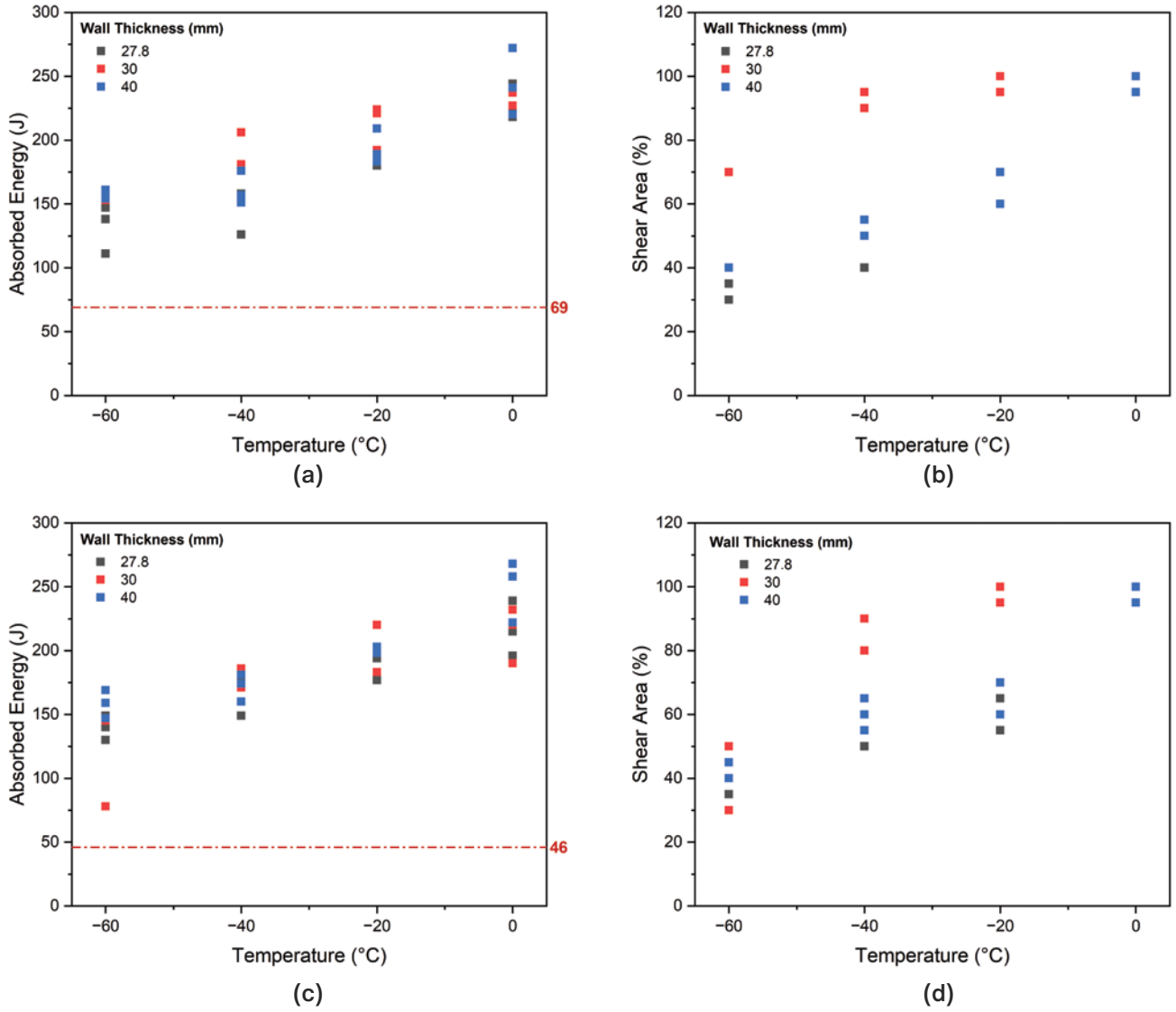

The values of absorbed energy and shear area fraction as a function of tested temperature are shown in Fig. 8. The data show results for pipes with WT of 27.8, 30 and 40 mm. The red dashed line indicates the minimum requirements for absorbed energy for offshore structural applications in longitudinal (69 J) and transverse (46 J) directions, respectively, according to DNV-OS-B101 and ABS Materials and Welding – Part 2. It is important to notice that these standards do not require minimum shear area.

All the results are above the minimum requirements for both test directions. All the results were achieved with a large safety margin, being just one value below 100 J for WT 30 mm and temperature of –60°C. The drop in the absorbed energy with the decrease in temperature is expected, but for this material the drop was not abrupt, being a potential candidate for the extremely low-temperature-environment applications as requested by the standards. This behavior can be attributed to the effective solid solution strengthening by nickel and copper, combined with the refined bainite microstructure with a fine and homogeneous distribution of precipitates along the matrix, as seen in Figs. 6e–6h.

Fig. 9 displays SEM images of the fracture surface features from CVN specimen tested at –60°C. The fracture modes found in the evaluated specimen are highlighted in Fig. 8a in a magnification of 80x using secondary electron detector. Figs. 9b, 9c and 9d correspond to different

Figure 9

Scanning electron microscopy (SEM) images highlighting the morphologies of the fracture surface after CVN impact test at -60°C: Ductile and brittle fracture (a), transition between the two fracture modes (b), dimples in ductile fracture (c) and cleavage in brittle fracture (d).

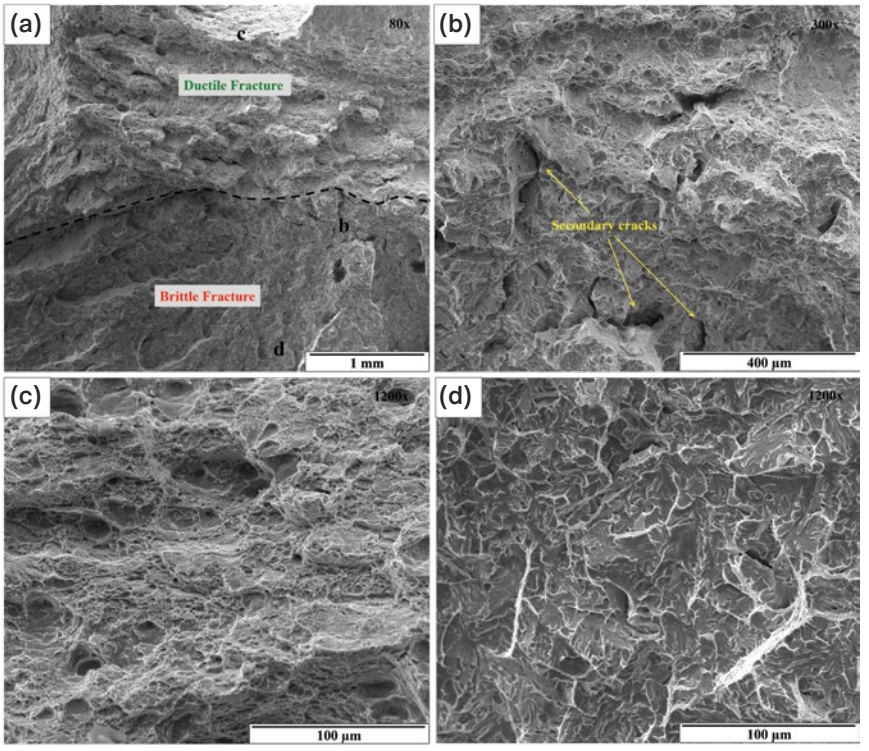

analyzed regions, as indicated by their respective letters in Fig. 9a.

It can be seen in Fig. 9a that both ductile and brittle fracture modes occur for this X100Q grade as is expected at such low temperature. Fig. 9b shows, in a higher magnification, the transition between the fracture modes, being possible to observe the presence of secondary cracks in the brittle region. Due to the very low temperature, the material embrittlement is expected mainly for body-centered cubic (BCC) steels, since the screw dislocations present in this crystal lattice do not have enough thermal activation to motion, which is the case of X100Q grade. Fig. 9c shows the dimples in ductile area where some plastic deformation has occurred, while in Fig. 9d it is possible to observe the cleavage along the crystallographic plan, indicating the occurrence of brittle fracture.

Conclusions

In this study, high-strength seamless pipes steel of X100Q grade were successfully obtained using a well-balanced alloy design by means of low-carbon and microalloying concept combined with a well-controlled manufacturing process of steelmaking, rolling and heat treatment to attend offshore structural applications worldwide. Tensile and hardness properties were achieved with a large safety margin for all the pipe dimensions evaluated, as well as impact toughness down to –60°C. The high strength combined with a suitable toughness at low temperatures can be attributed to a microstructure composed mainly by tempered bainite with few islands of tempered martensite, with fine precipitates homogeneously distributed along the matrix. Based on the results, the material represents a very promising product for offshore applications in harsh conditions, especially jack-up rigs and wind turbine installation vessels.

This article is available online at AIST.org for 30 days following publication.

References

1. Q. Yin, J. Yang, G. Xu, R. Xie, M. Tyagi, L. Li, X. Zhou, N. Hu, G. Tong, C. Fu and D. Pang, "Field Experimental Investigation of Punch-Through for Different Operational Conditions During the Jack-Up Rig Spudcan Penetration in Sand Overlying Clay," *Journal of Petroleum Science and Engineering,* Vol. 195, No. 107823, December 2020, pp. 1–21, https://doi.org/10.1016/j.petrol.2020.107823.
2. D. Ahn, S. Shin, S. Kim, H. Kharoufi and H. Kim, "Comparative Evaluation of Different Offshore Wind Turbine Installation Vessels for Korean West–South Wind Farm," *International Journal of Naval Architecture and Ocean Engineering,* Vol. 9, No. 1, January 2017, pp. 45–54, https://dx.doi.org/10.1016/j.ijnaoe.2016.07.004.
3. K. Ma, J. Kim, J. Park, J. Lee and J. Seo, "A Study on Collision Strength Assessment of a Jack-Up Rig With Attendant Vessel," *International Journal of Naval Architecture and Ocean Engineering,* Vol. 12, October 2019, pp. 241–257, https://dx.doi.org/10.1016/j.ijnaoe.2019.10.002.
4. Gas Outlook, "Gulf of Thailand Oil and Gas Exploration Faces Stubborn Hurdles," accessed 30 January 2025, https://gasoutlook.com/analysis/gulf-of-thailand-oil-and-gas-exploration-faces-stubborn-hurdles.

5. ABB, “ABB Wins System Contract for Japan’s First Super-Size Wind Turbine Installation Vessel,” accessed 30 January 2025, https://new.abb.com/news/detail/58205/abb-wins-system-contract-for-japans-first-super-size-wind-turbine-installation-vessel.
6. X. Qi, X. Wang, H. Di, X. Shen, Z. Liu, P. Huan, L. Chen, “Effect of Ti Content on the Inclusions, Microstructure and Fracture Mechanism of X100 Pipeline Steel Laser-MAG Hybrid Welds,” *Materials Science and Engineering A,* Vol. 831, No. 142207, January 2022, https://doi.org/10.1016/j.msea.2021.142207.
7. X. Qi, P. Huan, X. Wang, X. Shen, Z. Liu and H. Di, “Effect of Microstructure Homogeneity on the Impact Fracture Mechanism of X100 Pipeline Steel Laser–MAG Hybrid Welds With an Alternating Magnetic Field,” *Materials Science and Engineering A,* Vol. 851, No. 143656, August 2022, https://doi.org/10.1016/j.msea.2022.143656.
8. S. Cheng, R. Lv, F. Cheng, B. Han, A. Fu, X. Zhang, J. Zhang, Y. Feng and H. Gao, “Microstructure and Properties of X100 Large-Deformability Pipeline Steel Based on Heating On-Line Partitioning,” *Materials Today Communications,* Vol. 35, No. 105771, June 2023, https://doi.org/10.1016/j.mtcomm.2023.
9. S. Scherf, S. Harksen, R. Hojda, P. Lang, M. Schutz, A. Jahn and R. Nirello, “Advanced High Toughness X100 Seamless Pipes With a New Specialized Alloying Concept for Arctic Offshore Structurals Applications,” *Proceedings of the 27th International Ocean and Polar Engineering Conference,* San Francisco, Calif., USA, 2017.
10. S. Scherf, S. Harksen, R. Hojda and D. Stroetgen, “Weldability of High Toughness X100 Seamless Pipes With a New Low Carbon Alloying Concept for Arctic Offshore Structural Applications,” *Proceedings of the 28th International Ocean and Polar Engineering Conference,* Sapporo, Japan, 2018.
11. A. Jahn, S. Scherf, B. Koschlig, W. Wessel, D. Toma, G. Kubla, R. Hojda and R. Nirello, “Customized High Strength Seamless Pipes With Advanced Toughness for Offshore Constructions,” *Proceedings of the 25th International Ocean and Polar Engineering Conference,* Kona, Hi., USA, 2015.
12. Rules for Materials and Welding, Part 2, ABS, USA, 2022.
13. Offshore Standards – Metallic Materials, DNV-OS-B101, DNV, 2023
14. Standard Test Methods for Determining Hardenability of Steel, ASTM A255, ASTM International, USA, 2010.
15. Standard Test Methods and Definitions for Mechanical Testing of Steel Products, ASTM A370, ASTM International, USA, 2023.
16. Standard Test Methods for Notched Bar Impact Testing of Metallic Materials, ASTM E23, ASTM International, USA, 2023.
17. Standard Test Methods for Vickers Hardness and Knoop Hardness of Metallic Materials, ASTM E92, ASTM International, USA, 2023.

AISTech This paper was presented at AISTech 2025 — The Iron & Steel Technology Conference and Exposition, Nashville, Tenn., USA, and published in the AISTech 2025 Conference Proceedings.